DEVELOPMENT OF A COUPLED FINITE ELEMENT-DISCRETE ELEMENT CODE FOR SIMULATING SATELLITE BREAKUPS

Erkai Watson[(1)], Nathanaël Durr [(1)], José Luis Sandoval Murillo [(1)], Markus Büttner[(1)]

(1) Fraunhofer EMI, Ernst-Zermelo-Str. 4, 79104 Freiburg, Germany,
Email: erkai.watson@emi.fraunhofer.de

ABSTRACT

We present ongoing development of a coupled Finite Element Method (FEM) and Discrete Element Method (DEM) simulation code for modeling the breakup and fragmentation of spacecraft caused by hypervelocity impacts. We describe various coupling approaches and demonstrate the implemented coupling with basic material tests. Hypervelocity impact simulations are presented and compared with experimental data to highlight the advantages and necessity of a coupled FEM-DEM approach.

1 INTRODUCTION

The increasing number of objects in orbits constitute a growing risk to satellites operating around Earth. As the number of objects grow, the probability of catastrophic collisions between orbiting objects increases. A key to understanding the space debris environment is an accurate modeling of the physical process of in-orbit satellite breakup and the resulting fragmentation. Traditionally, satellite breakups have been modeled using empirical models based on ground-based experiments and on-orbit observations, such as the NASA Standard Satellite Breakup Model (SSBM) [1]. These models provide useful information about fragment distributions, but as satellite materials evolve and researchers seek more refined predictions, there is increasing recognition of the need for more accurate, higher-fidelity models [2]–[4].

Numerical simulations are another solution to studying the physics of satellite breakup and predicting the characteristics of the ensuing fragments. Hydrocodes, which use Finite Element Method (FEM) codes coupled with particle methods, are often employed for modeling spacecraft breakups, given the extreme deformations involved. One example is the coupling of FEM with Smoothed Particle Hydrodynamics (SPH) for modeling the Cosmos-Iridium collision [5]. Other approaches combine FEM-SPH with finite element reconstruction to analyze fragment distributions [6] or couple FEM with mass points to simulate large satellite impact scenarios [7].

In our previous work, we studied the use of alternate simulation methods, specifically the Discrete Element Method (DEM), for modeling spacecraft breakup and fragmentation. DEM is well suited for modeling the transition from a solid material to a fragmented state, and therefore shows promise for modeling satellite breakups under HVI [8]. Previous work has shown excellent agreement between experimental and simulated fragment distributions for aluminum and CFRP satellites [9]–[11]. The shortcomings of our DEM simulation method stem from its extremely simple linear elastic constitutive model which is unable to capture more advanced material behavior, e.g. plasticity. This shortcoming is insignificant in areas of high shock loading, such as in the vicinity of a HVI event, but further away, the effects can be significant.

In this paper, we propose to remedy these shortcomings by coupling DEM with FEM, with DEM being used for areas of high shock loading, and FEM in all other areas. We describe the modeling approach used to couple these two numerical methods followed by some example simulations to demonstrate the coupling. Two sets of hypervelocity impact scenarios are simulated and compared to data published in literature.

2 MODELING OF FINITE-DISCRETE ELEMENT COUPLING

Our DEM model consists of a collection of particles connected via spring-bonds to form a solid material. The interaction is governed by contact and bond potentials. Further details on the model can be found in [8], [12].

In a FEM mesh, we speak of finite elements and nodes, and in a DEM mesh of particles and bonds. FEM nodes and DEM particles belong to the generic term "mass point". The FEM-DEM coupling provided in our code comprises two approaches that can be used individually or in parallel in a model: *ab initio* and on-the-fly. *Ab initio* coupling considers the coexistence of FEM and DEM meshes in the initial configuration, whereas on-the-fly coupling generates a DEM mesh as a result of eroding finite elements via a continuum mechanics-based criterion, usually a critical strain. In both approaches, the aim is to ensure that the transition from the FEM mesh to the DEM mesh is as smooth as possible, i.e. that the stresses and strains transition from one mesh to the other

Proc. 9th European Conference on Space Debris, Bonn, Germany, 1–4 April 2025, published by the ESA Space Debris Office
Editors: S. Lemmens, T. Flohrer & F. Schmitz, (http://conference.sdo.esoc.esa.int, April 2025)

with as few noticeable artifacts as possible.

In the following and for the sake of simplicity, the description of the FEM-DEM coupling is presented using the *ab initio* approach and a planar-symmetric (2D) structured rectangular mesh. Three variants are presented.

Figure 1 shows variant (a) of the FEM-DEM coupled mesh, where the part outlined in red represents the DEM system and the part in black the FEM mesh. In this example, an identical resolution has been selected for the FEM mesh and DEM particles, and hybrid FEM-DEM mass points (yellow with green outline) have been used at the interface of both meshes.

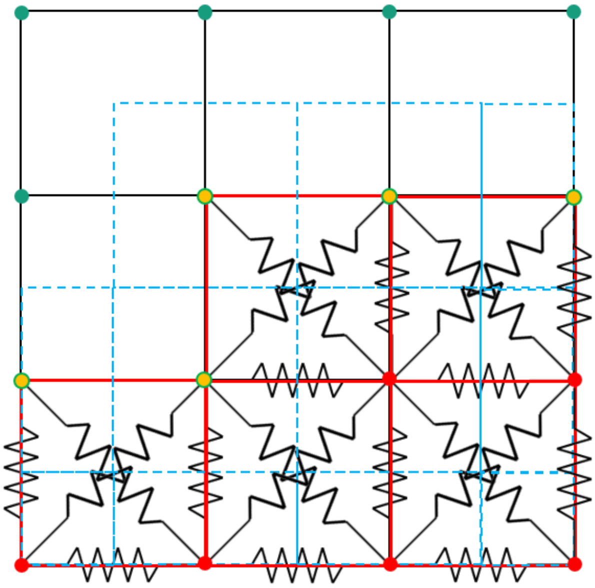

Figure 1. variant (a): the FEM-DEM coupling is achieved by using an identical resolution for the FEM and DEM meshes and using hybrid FEM-DEM mass points at the FEM-DEM interface.

In Figure 1, a pure FEM node (green) receives its forces in the classical way through the interaction with its attached finite elements. Similarly, a pure DEM particle (red) receives its force through its attached bonds. A hybrid mass point (yellow with green outline) receives its force from separate, summed contributions. The FEM force contribution comes from the connected finite elements while the DEM contribution comes only from the bond forces. In the DEM region, however, it should be noted that the particle volumes are not uniformly distributed, despite the regular mesh, but are subject to a distribution similar to that of the FEM mesh, which is indicated by the blue dashed frames in Figure 1.

A refined DEM resolution may be desirable if a specific area of the geometry is subjected to high stress leading to fragmentation that cannot be easily modeled using a FEM approach. To achieve this, variant (b) is a subdivision of the DEM domain carried out so that several DEM particles are located at the FEM-DEM interface and not exclusively on the FEM nodes, as seen in Figure 2. The DEM particles located at the FEM-DEM interface are referred to as support points.

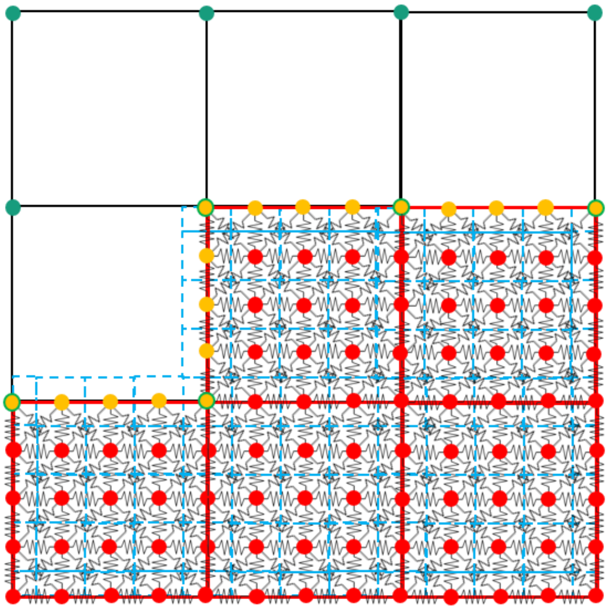

Figure 2. variant (b): the FEM-DEM coupling is achieved by using a finer resolution for the DEM mesh than the FEM mesh, and using hybrid FEM-DEM mass points and DEM support points.

In variant (a), the FEM-DEM coupling was based exclusively on hybrid mass points, which took on the dual function of FEM nodes and DEM particles. In variant (b), the coupling is extended to the support particles (yellow).

The interaction between the FEM domain and the DEM domain takes place in two steps. At the beginning of each time step, the kinematics of the FEM nodes determine the placement of the support particles. Forces are then calculated. Pure FEM nodes and pure DEM particles receive their forces according to the FEM and DEM approaches, respectively. Hybrid mass points receive their forces from the sum of the FEM and DEM contributions. Support particles, like pure DEM particles, receive their force exclusively from the pure DEM region, i.e. via bonds. At the end of each time step, the forces of the support particles (yellow) are fed back into the FEM nodes. This is done using a weighted sum of the support point forces, where the weighting factors are defined by the classical FEM shape functions.

Nevertheless. variants (a) and (b) suffer from the fact that the DEM particles are not centered on the volumes they represent. This can cause difficulties when dealing with contact between boundary particles and secondary impacts as contact identification and the resulting contact force may not behave as expected. Therefore, a variant (c) is proposed in Figure 3. In this variant, DEM particles are seeded with a uniform volume distribution within the original FEM mesh and connected to the FEM mesh not via the FEM nodes, but via virtual DEM particles (yellow) placed inside the FEM mesh, see Figure 3. Here, the FEM nodes are not hybrid since no bonds connect them to the DEM mesh.

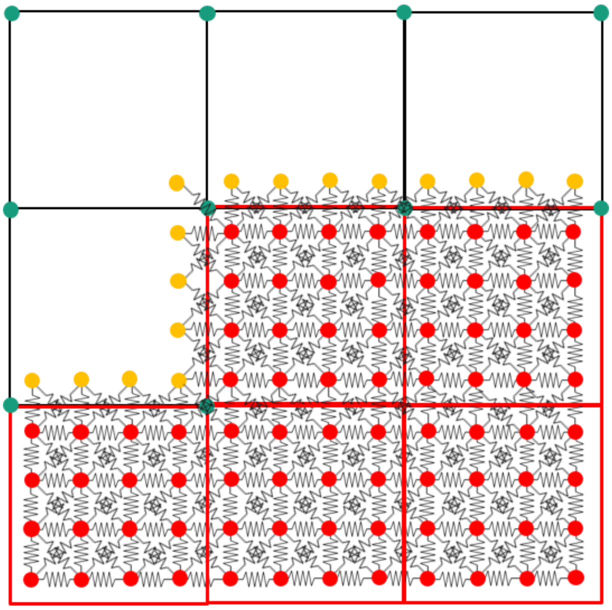

Figure 3. variant c: the FEM-DEM coupling is achieved by using a finer resolution for the DEM mesh than the FEM mesh, using virtual DEM particles, and removing the hybrid nature of interface FEM nodes.

The virtual DEM particles are, similar to variant (b), seeded with respect to the kinematics of the FEM mesh and interact with the real DEM particles via bonds. But in contrast to variant (b), the weighted sum of their forces is not only fed back to the FEM nodes located at the interface of the FEM and DEM meshes, but to all nodes of the elements in which they are embedded. However, since the closer the node, the higher the force contribution, the interface FEM nodes receive the highest force contribution from the virtual DEM particles.

The description given above for the *ab initio* coupling can be transposed to the on-the-fly coupling. The only difficulty for the latter lies in the determination of the force-stretch law for new bonds that are no longer in equilibrium due to previous deformations of the FEM mesh. Since the DEM model represents the hydrostatic loads well, a convenient method consists in extracting the 3D volumetric strain ε_{vol} of the eroding FEM element and stating that its third equals the 1D stretch s of the newly formed bonds. Knowing the instantaneous length r of a new bond due to the geometry of the eroding element, its initial bond length r_0 can be reconstructed using this formula:

$$r_0 = \frac{r}{1+s} = \frac{r}{1+\frac{\varepsilon_{vol}}{3}}. \tag{1}$$

This allows the conversion of a pre-stressed FEM element into a series of pre-stretched DEM systems of bonds and particles.

3 FINITE-DISCRETE ELEMENT COUPLING EXAMPLES

Implementation of the FEM-DEM coupling is currently still under development. In this section we show some preliminary results that have been implemented with variant (a) shown in Figure 1.

A good indicator for a successful FEM-DEM coupling is the observation of a propagating longitudinal wave in a material that is half meshed with FEM and half with DEM. If no reflecting wave occurs at the FEM-DEM transition zone, the FEM-DEM coupling can be considered successful.

Figure 4a show a block of aluminum discretized *ab initio;* the left half with FEM and the right half with DEM. A constant 20 m/s velocity boundary condition is applied to the left face. The rear right face is unconstrained. Other faces are constrained except in the direction of the velocity boundary condition.

A measurement tracer, placed in the aluminum block show in yellow in Figure 4b, measures the local velocity of the material. Figure 4b shows the velocity data of the passing and reflecting longitudinal wave for three different cases: a) FEM only, where the entire aluminum block is discretized with FEM, b) DEM only, where the entire aluminum block is discretized with DEM, and c) FEM-DEM where the block is discretized as shown in Figure 4a. The material properties of the DEM and FEM models are chosen such that the longitudinal wave speeds match.

Figure 4b shows the propagation of the longitudinal wave past the measurement tracer. The initial compressive wave passes at 0.25 µs, the reflected rarefaction wave returns at 1µ, and is again reflected back as a compressive wave passing at 1.5 µs, continuing back and forth. Although the coupled FEM-DEM wave trace does show some effects of disruption at the interface after a few oscillations, the initial few transitions between FEM and DEM show virtually no effect of crossing the interface.

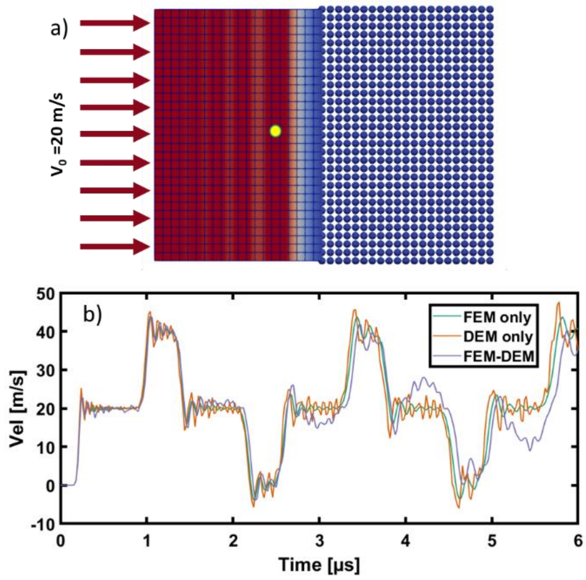

Figure 4. Wave propagation between FEM-DEM interface.

In Figure 5 we show a small qualitative example of the on-the-fly conversion of from FEM to DEM. At t_0, a small cluster of DEM particles impacts against a larger block of DEM-FEM material. Upon impact, a stress wave propagates through the DEM and into the FEM. The stress wave deforms the FEM beyond a critical strain, triggering the conversion to DEM. This can be seen at t_1 in Figure 5, where the first two rows of finite elements have been converted to particles.

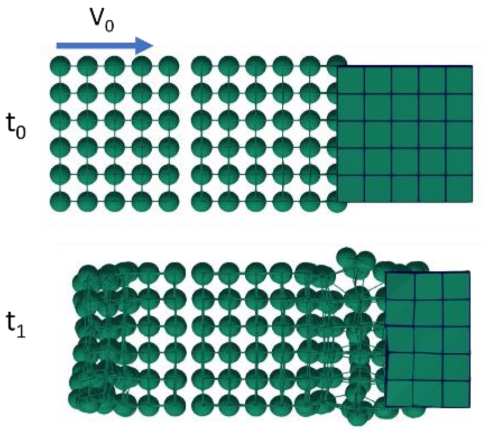

Figure 5. On-the-fly conversion of FEM to DEM.

4 HYPERVELOCITY IMPACT EXAMPLES

We present two sets of hypervelocity impact simulations that demonstrate the usefulness and necessity of the FEM-DEM coupling: a hypervelocity impact of aluminum spheres on thin plates and the simulation of a mock-up satellite catastrophic breakup.

4.1 Sphere on Plate Impacts

We simulate two sphere-plate hypervelocity impact experiments described in literature [13]. Parameters of the two experiments are shown in Table 1.

Table 1:Experimental parameters from [13].

Num.	Sphere Diameter [mm]	Target Thickness [mm]	Witness Plate Thickness [mm]	V_0 [km/s]
Exp 4	6.35	0.5	2	4.24
Exp 20	6.35	2	2	5.26

As the actual coupling described in sections 2 and 3 are still underdevelopment, we use of a hybrid, instead of coupled, DEM-FEM approach for the impact simulations. The approach, as described in our previous work [14], involves using the DEM for discretizing the sphere and the target plate and FEM for discretizing the witness plate. The simulations are run sequentially. First the DEM simulation of the sphere-target plate impact is run, resulting in a debris cloud of aluminum fragments. These fragments are imported into the FEM simulation as mass points for the second half of the simulation, the interaction of the debris cloud with the witness plate.

Figure 6 and Figure 7 show comparisons of the DEM portion of the simulation with the experimental images from [13]. Simulation and experimental images are not to scale.

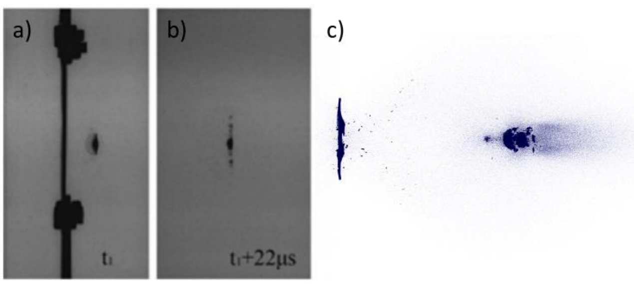

Figure 6. Comparison of debris cloud from Exp 4. a) and b) experimental images from [13], *c) simulation image*

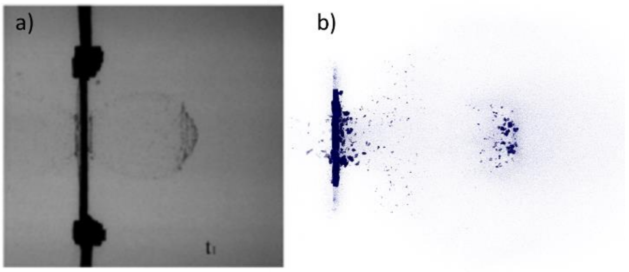

Figure 7. Comparison of debris cloud from Exp 20. a) experimental images from [13], *b) simulation image*

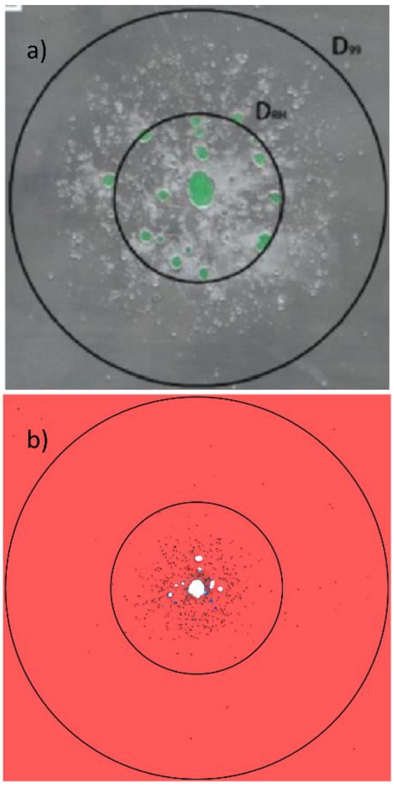

Figure 8. Comparison of experimental (a) and simulated (b) witness plate of Exp. 4. Experimental image from [13].

Figure 8 and Figure 9 show a comparison between experimental and simulated witness plates. Reference [13] defines a diameter of annular damage D_{RH} and main damage diameter D_{99}. These are transferred in their original diameters the simulated images to serve as guides to the eye for comparison.

Considering Figures 6-9, we can see that the simulation is more able to accurately predict the fragmentation and damage in the witness plate for Exp 20 than for Exp 4. In Figure 6, we can see a small spall bubble forming behind the sphere, while in contrast, the simulated sphere remains relatively intact. Correspondingly, in Figure 8, we see that the number of craters and damaged area in the simulation are less than the that in the experiments. This is due to the less fragmented nature of the simulated sphere.

The simulation results of Exp. 20, in contrast, is much closer to those of the experiment. In Figure 7, we see a much better match in term of fragmentation between simulation and experiment, while in Figure 9 the number of perforations, as well as the damaged area matches the experiment rather well.

The primary difference between these two simulations is the t/D ratio, the ratio of the plate thickness to projectile diameter. In Exp 4, t/D=0.079, the shock wave induced in the sphere becomes attenuated by a reflected rarefaction wave before completely propagating through the sphere. This leads to regions of material that experience a reduced shock loading [15]. If the loading becomes too weak, many of the simplifying assumptions built into the model no longer hold and the results deviate from reality [8]. In Exp 20, t/D=0.315, the shock wave is able to propagate through the sphere without being attenuated and the simulated results match the experiment much more closely.

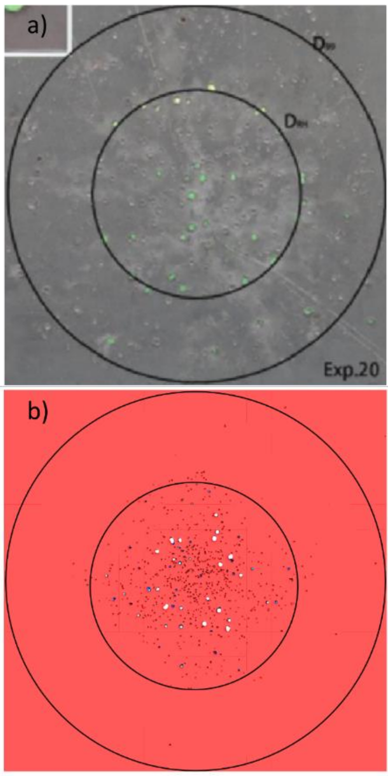

Figure 9. Comparison of experimental (a) and simulated (b) witness plate of Exp. 20. Experimental image from [13].

4.2 Satellite Breakup Simulation

We simulate a mock-up satellite breakup experiment found in literature [16] and compare the resulting damage and fragment distribution curves. The experimental mock-up satellite in shown in Figure 10. It consists primarily of aluminum, with some steel hardware and printed circuit boards (PCB) inside 19 aluminum electronic boxes. The entire satellite weight about 7.3 kg and measures 40 cm × 40 cm × 40 cm [16]. The satellite is impacted by a 97g conical aluminum projectile traveling at 3.26 km/s.

We model this small satellite using our DEM code as closely as possible. Many dimensions had to be assumed from lack of details specified in the publication. Figure 11 shows the DEM model. Aluminum is shown in red, purple, and orange. Steel connecting pieces are shown in green, and PCBs inside the electronic boxes are shown in blue. Some plates and electronic boxes have been removed for visualization. The impact location is not specified in the original publication, so one location was arbitrarily chosen. The model was discretized with 22.8 million particles.

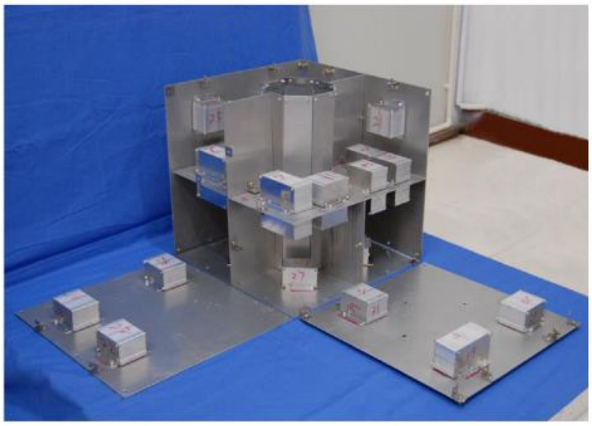

Figure 10. Mock-up satellite used in impact experiment. Image from [16].

Fehler! Verweisquelle konnte nicht gefunden werden. shows the satellite 2.6 ms after impact. The satellite undergoes a catastrophic breakup after the impact with an energy to mass ratio of 71 J/g. An experimental post-analysis of the fragmentation is shown in Figure 13. There are many similarities that can be seen between the resulting simulation and experimental fragments. In the Figure 13a we see that all the outer plates have become torn apart from the each other. This also occurs in the simulation. In both experiment and simulation, we can see that of the outer plates, the side facing the impact has a small hole, the side away from the impact is severely fragmented (not shown in Fig a, assumed to be fragmented), and that the upper and lower side plates (+Z and -Z) suffered more damage than the less exposed side plates (+Y and -Y). Differences are apparent in the survivability of the 19 electronic boxes, with the experiment showing primarily broken boxes, while the simulation shows more intact boxes. This difference could be due to the unknown properties of the boxes, such as thickness and joining technique. In the simulation the electronic boxes are seamlessly made from a single material instead of being bolted together, probably giving them a greater rigidity than in the experiment.

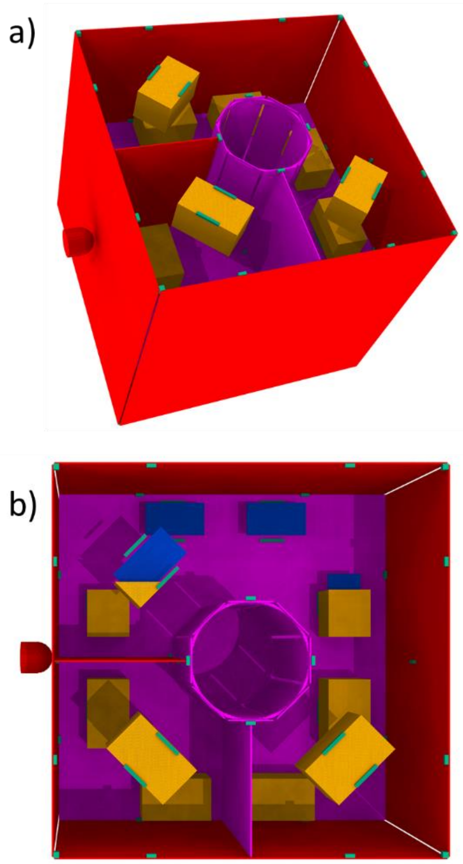

Figure 11. DEM model of mock-up satellite shown in Figure 10.

Figure 13 shows the cumulative fragment distribution of the satellite impact, comparing the simulation results to the experimental results. The predictions of the NASA Standard Satellite Breakup Model (SSBM) [1] are included for reference. Overall, the shape of the distribution from the simulation matches the experimental size distribution very well. The deviation for L_c < 0.002 m is due to the rather large discretization size. Individual discrete particles have a diameter of 0.5×10^{-4} m. The deviation and gradual change of slope beginning around L_c = 0.002 m represent the resolution limit of this particular simulation. The deviation between simulation and experiment at 0.002 m < L_c < 0.02 m is likely caused by unknow geometry, impact location, and impact direction in the experiment, all of which strongly effect the number of electronic boxes directly impacted inside the satellite, and therefore the number of smaller fragments generated.

The discretization size is also likely to influence the size distribution of the smaller fragments. Although this satellite was modeled with 22.8 million particles, this only equates to a 0.5 mm particle size. The satellite is almost entirely modeled with 1.5 mm thick aluminum, meaning only three particles can fit within the thickness of the aluminum sheet. This severely limits the fragmentation in the thickness direction of the material, potentially leading to some deviation in the total fragment number. Our previous simulations of satellite breakup have focused on smaller and simpler satellites allowing smaller discretization sizes hence more particles through the wall thickness, which in turn leads to more accurate fragment distributions [10][17].

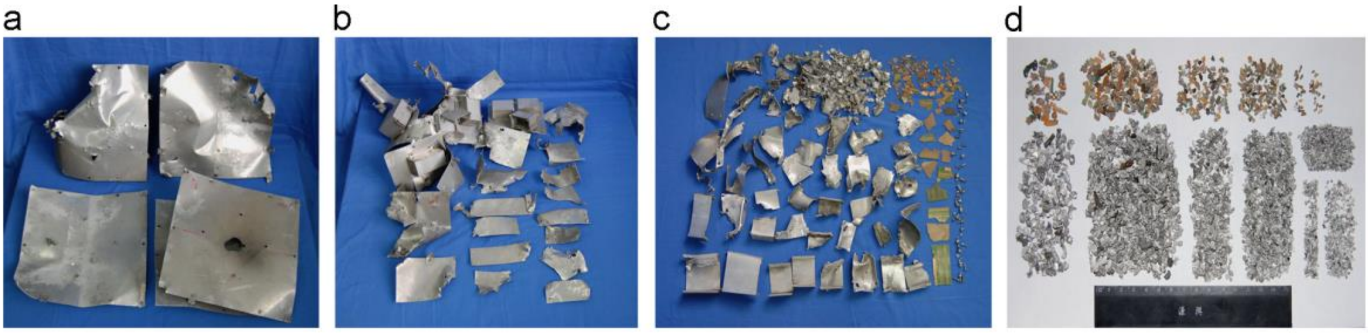

Figure 12. Post-analysis fragment analysis of mock-up satellite. Image from [16].

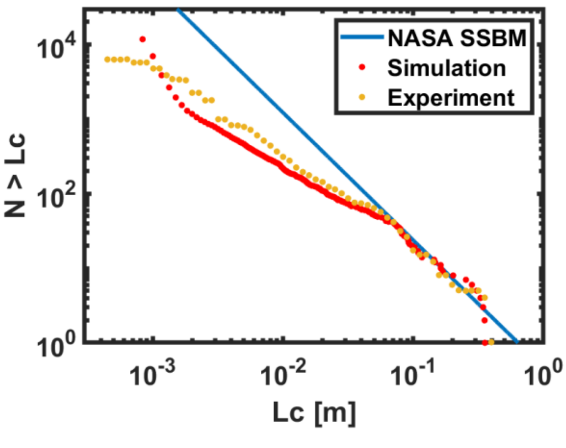

Figure 13. Cumulative fragment distribution of mock-up satellite. Experimental data from [16].

This satellite simulation illustrates one of the primary reasons why a coupling of DEM and FEM is needed. With the goal of simulating larger satellites, the problem encountered with discretizing thin structures becomes more acute. FEM, in contrast to our DEM implementation, is much better suited to modeling large thin structures undergoing large deformations (but not fragmentation) in a computationally efficient manner. In the simulation of **Fehler! Verweisquelle konnte nicht gefunden werden.**, large portions of the satellite remain completely intact and could be effectively modeled with FEM, with only selected areas that undergo fragmentation to be modeled with a finely resolved DEM.

5 CONCLUSIONS

By coupling the Discrete Element Method (DEM) with the Finite Element Method (FEM), we aim to extend the capabilities of satellite breakup simulations by capitalizing on the strengths of each method. Different modeling approaches are presented for coupling FEM and DEM, with the goal of an efficient and smooth interaction between meshed finite elements and discrete particles. One of these coupling variations has been implemented to date. We investigate the implemented coupling method by examining the passage of a longitudinal wave through material modeled with the coupled FEM-DEM showing good results.

Hypervelocity impact simulations are compared with experiments from literature and illustrate scenarios where coupled FEM-DEM simulations would be very beneficial. We examine hypervelocity impacts into thin plates, modeling the fragmentation with DEM and the cratering in a rear witness plate with FEM. Results show that the two methods working in conjunction can lead to good results. We also study the breakup of a mock-up satellite, comparing the DEM simulated fragment distribution to fragment distribution collected from the experiment. This example illustrates the need for an FEM coupling as we strive to model larger satellite breakup events. Ongoing work focuses on completing the implementation of the FEM-DEM coupling and applying it to the study of more complex fragmentation problems.

10.1115/hvis2022-57.

6 REFERENCES

[1] N. L. Johnson, P. H. Krisko, J. C. Liou, and P. D. Anz-Meador, "NASA's new breakup model of EVOLVE 4.0," *Adv. Sp. Res.*, vol. 28, no. 9, pp. 1377–1384, 2001, doi: 10.1016/S0273-1177(01)00423-9.

[2] M. Nishida, H. Kato, K. Hayashi, and M. Higashide, "Ejecta size distribution resulting from hypervelocity impact of spherical projectiles on CFRP laminates," *Procedia Eng.*, vol. 58, pp. 533–542, 2013, doi: 10.1016/j.proeng.2013.05.061.

[3] K. Sakuraba, Y. Tsuruda, T. Hanada, J. C. Liou, and Y. Akahoshi, "Investigation and comparison between new satellite impact test results and NASA standard breakup model," *Int. J. Impact Eng.*, vol. 35, no. 12, pp. 1567–1572, 2008, doi: 10.1016/j.ijimpeng.2008.07.068.

[4] H. Cowardin *et al.*, "Updates on the Debrisat Hypervelocity Experiment and Characterization of Fragments in Support of Environmental Models," *Proc. 16th Hypervelocity Impact Symp. HVIS 2022*, vol. 180, pp. 1–11, 2023, doi: 10.1115/hvis2022-8.

[5] H. K. Springer, W. O. Miller, J. L. Levatin, A. J. Pertica, and S. S. Olivier, "Satellite Collision Modeling with Physics-Based Hydrocodes : Debris Generation Predictions of the Iridium-Cosmos Collision Event and Other Impact Events," *Sp. Situational Aware.*, no. November 2014, 2010.

[6] X. T. Zhang, G. H. Jia, and H. Huang, "Finite element reconstruction approach for on-orbit spacecraft breakup dynamics simulation and fragment analysis," *Adv. Sp. Res.*, vol. 51, no. 3, pp. 423–433, 2013, doi: 10.1016/j.asr.2012.09.023.

[7] M. Schimmerohn *et al.*, "Numerical investigation on the standard catastrophic breakup criteria," *Acta Astronaut.*, vol. 178, no. January 2020, pp. 265–271, 2020, doi: 10.1016/j.actaastro.2020.09.014.

[8] E. Watson and M. Steinhauser, "Discrete Particle Method for Simulating Hypervelocity Impact Phenomena," *Materials (Basel).*, vol. 10, no. 4, p. 379, 2017, doi: 10.3390/ma10040379.

[9] E. Watson, N. Durr, J. L. S. Murillo, M. Büttner, and P. Matura, "Simulating Hypervelocity Impacts on Cfrp With a Discrete Element Approach," *Proc. 16th Hypervelocity Impact Symp. HVIS 2022*, pp. 1–12, 2023, doi:

[10] E. Watson, J. L. Sandoval Murillo, M. Büttner, P. Matura, and M. Schimmerohn, "Simulating Hypervelocity Impact with a Discrete Element Approach," *Acta Astronaut.*, vol. 199, pp. 425–435, Oct. 2022, doi: 10.1016/J.ACTAASTRO.2022.07.044.

[11] E. Watson, J. L. Sandoval Murillo, N. Durr, and N. Ledford, "Simulating impact-induced satellite breakups with a discrete element method," *Acta Astronaut.*, vol. 219, no. January, pp. 428–437, 2024, doi: 10.1016/j.actaastro.2024.03.032.

[12] S. Signetti *et al.*, "Pellet Shattering Process for the ITER Disruption Mitigation System – Part I: Development of a Discrete Element Code for Modeling the Dynamic Fragmentation of Cryogenic Materials (in press)," *2024 HVIS, ASME Proc. Ser. 2024 17th Hypervelocity Impact Symp.*

[13] K. Wen, X. W. Chen, R. Q. Chi, and Y. G. Lu, "Analysis on the fragmentation pattern of sphere hypervelocity impacting on thin plate," *Int. J. Impact Eng.*, vol. 146, no. September, p. 103721, 2020, doi: 10.1016/j.ijimpeng.2020.103721.

[14] E. Watson, R. Putzar, N. Durr, K. K. Sharma, J. L. S. Murillo, and M. Schimmerohn, "Shape Effect of Non-Spherical Projectiles on CFRP Spacecraft Structures (in press)," *2024 HVIS, ASME Proc. Ser. 2024 17th Hypervelocity Impact Symp.*

[15] A. J. Piekutowski, "Formation and Description of Debris Clouds Produced by Hypervelocity Impact," *NASA Contract. Rep. 4707*, 1996, doi: 10.1016/S0734-743X(01)00122-1.

[16] S. W. Lan, S. Liu, Y. Li, F. W. Ke, and J. Huang, "Debris area distribution of spacecraft under hypervelocity impact," *Acta Astronaut.*, vol. 105, no. 1, pp. 75–81, 2014, doi: 10.1016/j.actaastro.2014.08.011.

[17] E. Watson, J. L. Sandoval Murillo, N. Durr, and N. Ledford, "Simulating impact-induced satellite breakups with a discrete element method," *Acta Astronaut.*, vol. 219, no. March, pp. 428–437, 2024, doi: 10.1016/j.actaastro.2024.03.032.